

Optical feature extraction with illumination-encoded linear functions

Robin Gruna^a and Jürgen Beyerer^b

^aKarlsruhe Institute of Technology (KIT), Adenauerring 4, Karlsruhe, Germany;

^bFraunhofer Institute of Optronics, System Technologies and Image Exploitation, Fraunhoferstraße 1, Karlsruhe, Germany

ABSTRACT

The choice of an appropriate illumination design is one of the most important steps in creating successful machine vision systems for automated inspection tasks. In a popular technique, multiple inspection images are captured under angular-varying illumination directions over the hemisphere, which yields a set of images referred to as *illumination series*. However, most existing approaches are restricted in that they use rather simple patterns like point- or sector-shaped illumination patterns on the hemisphere. In this paper, we present an illumination technique which reduces the effort for capturing inspection images for each reflectance feature by using linear combinations of basis light patterns over the hemisphere as feature-specific illumination patterns. The key idea is to encode linear functions for feature extraction as angular-dependent illumination patterns, and thereby to compute linear features from the scene's reflectance field directly in the optical domain. In the experimental part, we evaluate the proposed illumination technique on the problem of optical material type classification of printed circuit boards (PCBs).

Keywords: Optical feature extraction, hemispherical illumination functions, reflectance fields, illumination series, material classification, multivariate image analysis, automated visual inspection

1. INTRODUCTION

The choice of an appropriate illumination design is one of the most important steps in creating successful machine vision systems for automated inspection tasks. Since in image acquisition all information about a scene is encoded in the reflected light field, the incident light field provided by the illumination must be able to reveal the information about a workpiece that is relevant to the inspection task. Particularly in real-time machine vision applications, where time is a major constraint, appropriate illumination can greatly simplify digital image processing tasks and improve their processing time and reliability. For instance, via an illumination that results in inspection images where defects are measured with high signal-to-noise ratio, simple image thresholding may suffice for defect detection, and computationally expensive and time consuming image processing algorithms can be avoided.

For many inspection tasks it is difficult or even impossible to find a single optimal illumination condition, and therefore, inspection images under multiple different illumination conditions have to be captured and analyzed. In a widely used technique, inspection images are captured under angular-varying illumination directions over the hemisphere, which yields a set of images referred to as *illumination series*.¹⁻³ However, most of the existing approaches from the literature are restricted in that they use rather simple and unspecific illumination patterns like point- or sector-shaped patterns on an illuminating hemisphere. As a consequence, many images with densely sampled illumination directions are needed to capture the reflectance properties of the workpiece under study. On the other hand, densely sampled illumination series are often highly redundant, since images of the same object obtained under similar illumination conditions are correlated.

In automated visual inspection, capturing illumination series with many images is problematic for two reasons: First, in many industrial applications there are severe constraints on inspection time, and hence it is desirable

Further author information: (Send correspondence to R.G.)

R.G.: E-mail: robin.gruna@kit.edu, Telephone: +49 (0)721 6091-263

J.B.: E-mail: juergen.beyerer@iosb.fraunhofer.de, Telephone: +49 721 608-45911

to capture and process as few inspection images as possible. Second, large illumination series lead to high-dimensional reflectance features that must be evaluated. However, from statistical learning theory it is known that the complexity of any classification problem grows with the number of input features. As a consequence, more training examples are needed to train a classifier due to the *curse of dimensionality*.⁴ In order to reduce the dimensionality of the feature space, methods from feature subset selection have been applied to determine the informative illumination directions for a given inspection task. Jehle et al.⁵ used a random forest classifier to learn optimal illumination directions for material classification by using embedded feature selection. A completely unsupervised approach to reduce the dimensionality of illumination series is presented by Gruna et al.,⁶ where redundant illumination directions are eliminated using spectral clustering.

In this paper, we aim to reduce the effort for capturing the reflectance properties of an object by using problem-specific extended patterns over the illuminating hemisphere. The key idea is to encode linear functions for feature extraction as angular-dependent illumination patterns, and thereby to compute features from the scene’s reflectance field directly in the optical domain. To this end, we first need to model image formation under arbitrary extended hemispherical illumination directions.

Modeling the appearance of objects under different illuminating directions has long been an active research area in both machine vision and computer graphics^{7,8}. In traditional approaches, the geometry and the material properties of an object are described by separate models, e.g., by a CAD model and a *Bidirectional Reflectance Distribution Function (BRDF)*, which is a function of incident and reflected light directions, specified in a local coordinate frame at the object’s surface. However, measuring the BRDFs of real-world objects can be very difficult if the object’s geometry is complex or not known in advance. An alternative to modeling the shape and the material properties of an object explicitly is to capture the appearance of the object directly. That is, the direct relationship between an incident illuminating light field and the light field reflected off the scene is modeled. This model is referred to as the *reflectance field*⁹ of the scene. As such, the reflectance field describes the light transport between illuminating and outgoing light field, and it includes all global illumination effects like interreflections, shadows or subsurface light scattering.

In our approach, we assume that the illuminating light field is distant, i.e., the incident illumination only varies directionally and thus is spatially constant across the illuminated object. Thus, we define the illuminating light field as function

$$L: \Omega^+ \rightarrow \mathbb{R}^+ \tag{1}$$

over the upper illuminating hemisphere $\Omega^+ := [0, \pi/2] \times [0, 2\pi)$, which describes the incident radiance ($[L] = \text{W}/\text{sr}\cdot\text{m}^2$) reaching the object from direction $\boldsymbol{\omega} := (\theta, \phi) \in \Omega^+$. In addition, we assume a fixed camera viewpoint which reduces the 4D reflected light field to a 2D projection, which can be parameterized on the camera sensor’s image plane.¹⁰

Since we represent the illuminating and the outgoing light field as 2D functions, the reflectance field becomes a 4D function $R(\boldsymbol{\omega}, \mathbf{x})$ where the outgoing illumination directions are parameterized in image pixel coordinates $\mathbf{x} \in [0, n_1] \times [0, n_2] \subset \mathbb{Z}^2$. For the camera, we assume a linear response so that image gray levels are proportional to the irradiance received by the sensor. Then, the grayscale image $g(\mathbf{x}, L(\boldsymbol{\omega}))$ captured under the hemispherical illumination function $L(\boldsymbol{\omega})$ is

$$g(\mathbf{x}, L(\boldsymbol{\omega})) = \int_{\Omega^+} R(\boldsymbol{\omega}, \mathbf{x})L(\boldsymbol{\omega}) \, d\sigma(\boldsymbol{\omega}), \tag{2}$$

where the 4D reflectance field $R(\boldsymbol{\omega}, \mathbf{x})$ of the imaged scene describes the light transport between incident illumination directions and image pixels.

2. CATADIOPTRIC ILLUMINATION DEVICE

In order to capture illumination series with extended illumination patterns over the hemisphere, we developed a catadioptric illumination device which is shown schematically in Figure 1a. The device is able to image small objects with a diameter up to 20 mm under arbitrary hemispherical illumination patterns. To this end, the

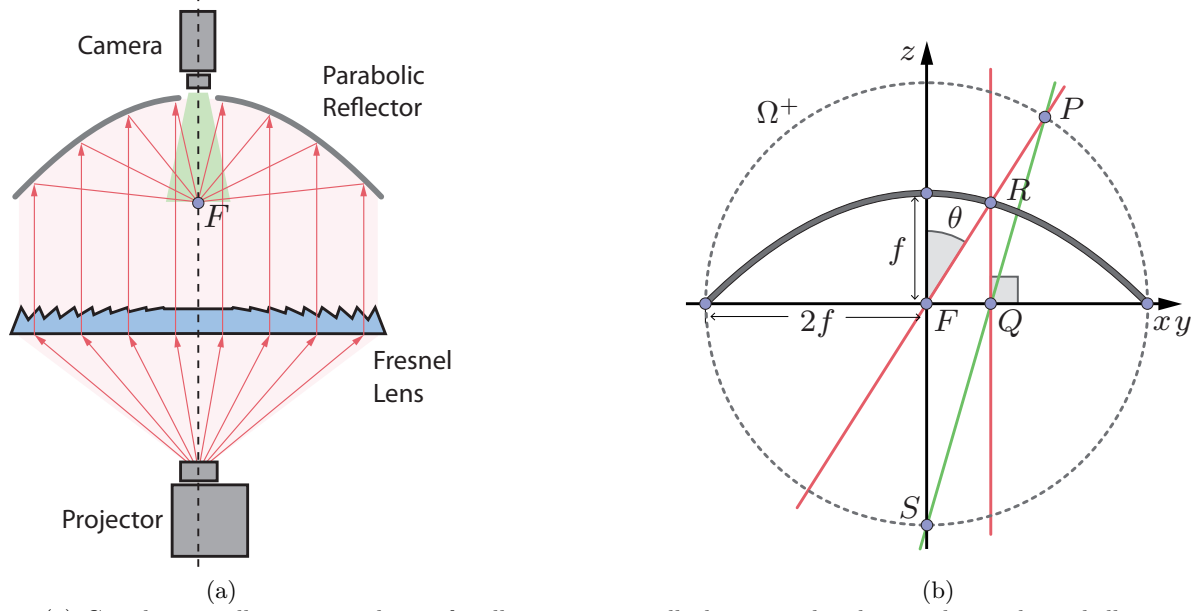


Figure 1. (a) Catadioptric illumination device for illuminating small objects with arbitrary hemispherical illumination patterns. A digital LCD projector, a Fresnel lens, a parabolic reflector with a center hole and a digital camera are aligned along their optical axes. By placing the optical center of the projector at the focal point of the Fresnel lens, all emitted light rays intersect at the focal point F of the reflector. (b) Schematic x - z -section through the parabolic reflector's center F . A ray QR parallel to the parabola's axis is reflected to the ray RF incident to the focal point F of the parabola. A point P on the hemisphere Ω^+ can be mapped to the corresponding point Q on the projector image plane (x - y -plane) by *parabolic projection* (red lines) or via *stereographic projection* (green line) from the sphere's south pole S .

object is placed at the focal point of a parabolic mirror and is illuminated by a digital light projector. At the same time, we capture high dynamic range images of the object from a fixed camera position. Jehle et al.⁵ use a very similar device in their work. However, our device, developed independently, differs in a wax coating of the parabolic mirror to obtain a more homogeneous illumination of the object under study.

The projector serves as programmable light source that allows controlling the relative radiance along the emitted light rays independently. In our experiments, we used a colorimeter* to linearize the projector's intensity transfer function. Assuming a pinhole model for the projector, each projector pixel can be thought of as source of individual light rays that diverge from the optical center of the projector. By placing the projector at the focal point of the Fresnel lens, the diverging light rays from the projector are converted into parallel rays and so an orthographic projection system is obtained.

The parabolic reflector is then used to transform the orthographic light field. Since the projected light field is parallel to the optical axis of the reflector, the light rays are reflected so that they intersect at the focal point F of the parabolic reflector. Since the parabolic reflector can be described by a regular paraboloid, and incident and reflected light rays are coplanar with the optical axis, only a planar cross-section of the reflector must be considered (see Figure 1b). We establish a Cartesian coordinate system with its origin at the focal point F of the parabolic reflector and its z -axis aligned with the optical axis of the device, pointing into the direction of the camera. Hence, the surface of the parabolic mirror can be described by the graph

$$\{(x, y, z): f - \frac{x^2 + y^2}{4f} - z = 0\}, \quad (3)$$

where f denotes the focal length of the reflector.

A x - z -slice through the parabolic reflector is schematically illustrated in Figure 1b. We refer to the x - y -plane as the *projector image plane* of the orthographic projection system and identify points in this plane by projector

*Datacolor Spyder3Elite™

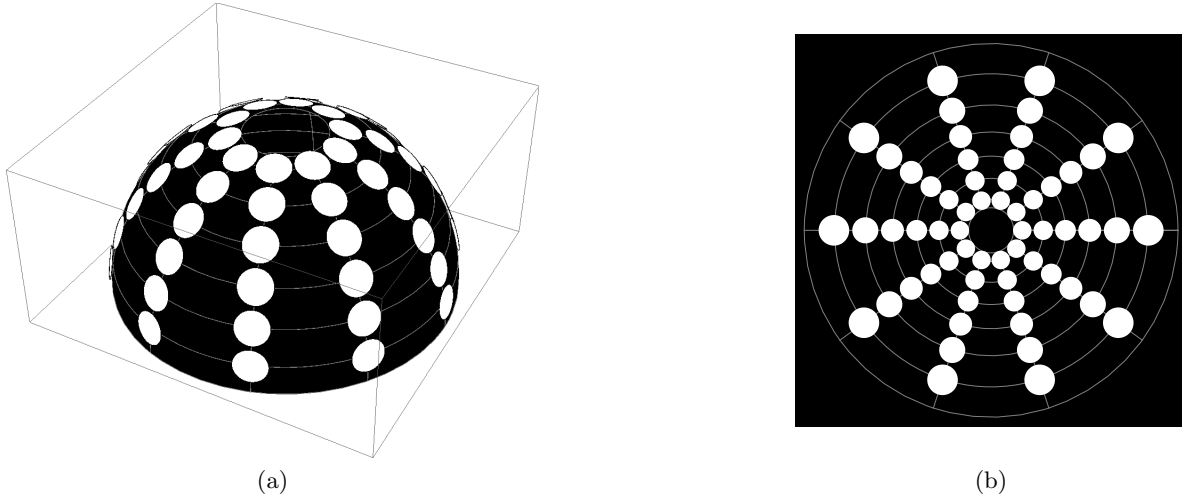


Figure 2. (a) Impulse-like illumination patterns on the hemisphere. (b) Parabolic projection of the hemispherical illumination pattern shown in (a). Since the parabolic projection is conformal, the shape of circles are conserved, however, their radii increases with increasing polar angle.

pixel coordinates. A light ray from the projector pixel Q parallel to the optical axis is reflected at R and passes through the focal point F . In order to illustrate the fact that the illumination device is able to produce arbitrary hemispherical illumination patterns $L(\omega)$, we consider the upper hemisphere of illumination directions Ω^+ that has radius $2f$ and is centered at F . Then there is a one-to-one correspondence between the ray QR , originating in the projector image plane, to the virtual light ray PF , originating at the point P on the hemisphere Ω^+ .

To physically generate arbitrary hemispherical illumination patterns, we need to transform the desired hemispherical light field $L(\omega)$ to the projector image plane. To this end, we consider the back-projection Q of the point P , which is the orthographic projection of the intersection R of the parabola and the virtual ray FP . This projection is referred to as *parabolic projection*¹¹ and can be used to parameterize directions over the hemisphere in a plane. Geyer et al.¹² showed, that the parabolic projection is equivalent to the well-known *stereographic projection*, which is also illustrated in Figure 1b.

To obtain a simple transformation rule for the parabolic projection, we identify points on the hemisphere Ω^+ using spherical coordinates, i.e., $P = (\theta, \phi)$ where $(\theta, \phi) \in \Omega^+$, and points in the projector image plane (x - y -plane) in polar coordinates, i.e., $Q = (\rho, \varphi)$ where $(\rho, \varphi) \in [0, 2f] \times [0, 2\pi)$. Since for the polar angle θ the following trigonometric relationship

$$\tan \theta = \frac{|FQ|}{|RQ|} = \frac{\rho}{f - \frac{\rho^2}{4f}} \quad (4)$$

is true, the transformation $\Phi: \Omega^+ \rightarrow [0, 2f] \times [0, 2\pi)$ from the illuminating hemisphere to the projector image plane can be expressed as

$$(\theta, \phi) \mapsto \left(2f \tan \frac{\theta}{2}, \varphi\right). \quad (5)$$

Note that due to the position of the camera, the polar angle θ in the presented device is limited to θ_{\min} to prevent a direct illumination of the camera. To sum up, we are able to produce arbitrary illumination patterns by emitting the parabolic projection of $L(\omega)$ to the projector image plane.

3. OPTICAL FEATURE EXTRACTION IN ILLUMINATION-SPACE

3.1 Image series with basis illumination patterns

An illumination series of the object under study with point-shaped illumination patterns provides our basis for computing a new set of problem-specific illumination patterns. For this purpose, we define an impulse-like

illumination basis function on the hemisphere. Let $\boldsymbol{\omega}_j = (\theta_j, \varphi_j)$ be a distant illumination direction on the hemisphere. Then, we define the impulse-like illumination function as

$$L_{\boldsymbol{\omega}_j}^{\text{rect}}(\boldsymbol{\omega}) := \text{rect}\left(-\frac{1}{2} + \frac{2d_A(\boldsymbol{\omega}, \boldsymbol{\omega}_j)}{\delta}\right), \quad (6)$$

where

$$d_A(\boldsymbol{\omega}_1, \boldsymbol{\omega}_2) := \arccos(\sin \theta_1 \sin \theta_2 \cos(\varphi_1 - \varphi_2) + \cos \theta_1 \cos \theta_2) \quad (7)$$

denotes the central angle distance between the two directions $\boldsymbol{\omega}_1$ and $\boldsymbol{\omega}_2$, and δ is the angular diameter of the illumination pattern as seen from the center of the illuminating hemisphere. By regularly sampling illumination directions from the illuminatable hemisphere and setting δ to a constant value, we obtain a set $\{L_{\boldsymbol{\omega}_j}^{\text{rect}}(\boldsymbol{\omega})\}_{j=1}^m$ of basis light patterns. Figure 2a shows a set of $m = 60$ impulse-like illumination patterns with unit radiance on the hemisphere.

We use the basis illuminations to sequentially illuminate the object under study and capture the image series $\{g(\mathbf{x}, L_{\boldsymbol{\omega}_j}^{\text{rect}}(\boldsymbol{\omega}))\}_{j=1}^m$ of congruent grayscale images.

These grayscale images can be stacked and interpreted as the m channels of a so-called *multivariate image*, where each channels is associated with a basis illumination pattern. Thus, each image pixel contains a m -dimensional vector of measured intensities. The multivariate image is considered as three-dimensional $n_1 \times n_2 \times m$ data structure, where two spatial dimensions represent the $n_1 \times n_2$ pixels in the image plane and the third dimensions represents the m variable illumination conditions. In this work, we do not consider spatial pixel correlations and discard all spatial information. Thus, we can unfold the $n_1 \times n_2$ -pixel images of the illumination series into column vectors \mathbf{g}_j , $j = 1, \dots, m$ with dimension $n = n_1 n_2$ and express the multivariate image data as two-dimensional $n \times m$ matrix $\mathbf{G} = [\mathbf{g}_1, \mathbf{g}_2, \dots, \mathbf{g}_m]$. In the following, we consider each image pixel, i.e., each matrix row vector \mathbf{g}_i^T , as an object (or sample), while we consider each matrix column \mathbf{g}_j as particular feature (or variable) of the objects. Since we are dealing with illumination series, a matrix row \mathbf{g}_i^T contains all the measured reflectance features under the different illumination conditions for pixel \mathbf{x}_i . By representing the illumination series as data matrix \mathbf{G} , multivariate statistical techniques can be used for illumination series analysis.¹³

3.2 Feature extraction in illumination-space

Illumination series contain large amounts of information regarding the reflectance properties of the illuminated objects. However, images of the same object obtained under similar illumination conditions are likely correlated and thus, densely sampled illumination series are highly redundant. Therefore, an obvious first step in the analysis of illumination series is to perform some type of dimensionality reduction or feature extraction to extract low-dimensional reflectance features.

Given the multivariate image data $\mathbf{G} \in \mathbb{R}^{n \times m}$, dimensionality reduction can be achieved by a linear transformation $\mathbf{W} \in \mathbb{R}^{m \times l}$ that maps the pixel feature vectors \mathbf{g}_i^T in the m -dimensional feature space to $\tilde{\mathbf{g}}_i^T$ in the l -dimensional (with $l < m$) reduced features space:

$$\tilde{\mathbf{g}}_i^T = \mathbf{g}_i^T \cdot \mathbf{W}, \quad i = 1, \dots, n. \quad (8)$$

In multivariate data analysis, the entries in the new constructed feature vector $\tilde{\mathbf{g}}_i^T$ are called *latent variables*. These combine and compress the original variables in order to fulfill certain mathematical properties that are useful for data analysis, e.g., the optimal representation of the original objects in the latent variable space or the optimal separation of given object classes. Linear latent variables are defined by a *loading vector*, which are the column vectors \mathbf{w}_k , $k = 1, \dots, l$ in \mathbf{W} . Equation (8) can be geometrically interpreted as projection of the multivariate data onto the linear sub-space spanned by the loading vectors. The projection coordinates are then referred to as the *scores* of the latent variables.

Equation (8) can be written as a single matrix equation

$$\tilde{\mathbf{G}} = \mathbf{G} \cdot \mathbf{W}, \quad (9)$$

where the obtained scores form the score matrix $\tilde{\mathbf{G}} \in \mathbb{R}^{n \times l}$ with reduced dimensionality. Now the score matrix can be folded back to a three-dimensional data structure with dimensions $n_1 \times n_2 \times l$, so that the matrix columns $\tilde{\mathbf{g}}_k$ can be interpreted as so-called *score images*. Each image pixel in the score image now contains a new feature vector with reduced dimension. Depending on the aim of multivariate image analysis, the score images can be constructed to have desired properties with regard to subsequent analyzing steps.

From Equation (9) it is clear, that the columns $\tilde{\mathbf{g}}_k$ of $\tilde{\mathbf{G}}$ are linear combinations

$$\tilde{\mathbf{g}}_k = \sum_{j=1}^m w_{jk} \mathbf{g}_j, \quad k = 1, \dots, l \quad (10)$$

of the columns of \mathbf{G} . By folding the vectors back to images, the score image can be written as linear combination of the illumination series according to

$$\tilde{g}_k(\mathbf{x}) = \sum_{j=1}^m w_{jk} g(\mathbf{x}, L_{\omega_j}^{\text{rect}}(\boldsymbol{\omega})). \quad (11)$$

Equation (11) indicates that the score image $\tilde{g}_k(\mathbf{x})$ is computed in *image-space*, that is, as linear combination of a previously recorded illumination series.

However, the computation of score images can also be performed directly in *illumination-space* by utilizing the linearity of light transport. This becomes apparent when we substitute Equation 2 into Equation 11 and interchange the sum and the integration:

$$\tilde{g}_k(\mathbf{x}) = \sum_{j=1}^m w_{jk} \int_{\Omega^+} R(\boldsymbol{\omega}, \mathbf{x}) L_{\omega_j}^{\text{rect}}(\boldsymbol{\omega}) d\sigma(\boldsymbol{\omega}) \quad (12)$$

$$= \int_{\Omega^+} R(\boldsymbol{\omega}, \mathbf{x}) \underbrace{\sum_{j=1}^m w_{jk} L_{\omega_j}^{\text{rect}}(\boldsymbol{\omega})}_{=: L_k^{\text{LC}}(\boldsymbol{\omega})} d\sigma(\boldsymbol{\omega}) \quad (13)$$

$$= g(\mathbf{x}, L_k^{\text{LC}}(\boldsymbol{\omega})).$$

This means, the score image $\tilde{g}_k(\mathbf{x})$ can be computed in the optical domain by encoding the loading vector \mathbf{w}_k as illumination pattern

$$L_k^{\text{LC}}(\boldsymbol{\omega}) := \sum_{j=1}^m w_{jk} L_{\omega_j}^{\text{rect}}(\boldsymbol{\omega}), \quad (14)$$

and by capturing the image $g(\mathbf{x}, L_k^{\text{LC}}(\boldsymbol{\omega}))$ of the illuminated object.

However, it is important to note that the linear combination in Equation (14) is under the restriction that the coefficients must be non-negative, i.e., $w_j \geq 0$, since it is not possible to emit illumination patterns with negative radiance. Therefore, we decompose the illumination pattern $L_k^{\text{LC}}(\boldsymbol{\omega})$ into two patterns

$$L_k^{\text{LC}}(\boldsymbol{\omega}) = L_k^{\text{LC}^+}(\boldsymbol{\omega}) - L_k^{\text{LC}^-}(\boldsymbol{\omega}) \quad (15)$$

where $L_k^{\text{LC}^+}(\boldsymbol{\omega}) := \sum_{j=1}^m w_{jk}^+ L_{\omega_j}^{\text{rect}}(\boldsymbol{\omega})$ encodes the positive and $L_k^{\text{LC}^-}(\boldsymbol{\omega}) := \sum_{i=1}^m w_{jk}^- L_{\omega_j}^{\text{rect}}(\boldsymbol{\omega})$ the negative coefficients, respectively. The new coefficients are then calculated as follows:

$$w_{jk}^+ := \begin{cases} w_{jk} & w_{jk} \geq 0 \\ 0 & \text{else} \end{cases} \quad \text{and} \quad w_{jk}^- := \begin{cases} 0 & w_{jk} \geq 0 \\ -w_{jk} & \text{else} \end{cases}. \quad (16)$$

The image under “negative” illumination is the computed by $g(\mathbf{x}, L_k^{\text{LC}}(\boldsymbol{\omega})) = g(\mathbf{x}, L_k^{\text{LC}^+}(\boldsymbol{\omega})) - g(\mathbf{x}, L_k^{\text{LC}^-}(\boldsymbol{\omega}))$ in image-space after the acquisition of the both images.

Due to the ability to encoding arbitrary linear functions \mathbf{w} and transformations \mathbf{W} as sets of illumination patterns, we can make use of multivariate techniques for linear feature extraction like principal component analysis (PCA), linear discriminant analysis (LDA) or non-negative matrix factorization (NMF) to compute problem-specific illumination patterns for automated visual inspection tasks. For that, we first need to capture an illumination series of the object under study with some basis illumination patterns. In an offline training stage, the linear transformations for feature extraction and the corresponding illumination patterns are computed in image-space. During online inspection, the computed illumination patterns are used to extract relevant reflectance features from the object under study in illumination-space. As consequence, due to shifting linear feature extraction into the optical domain, no complete illumination series has to be captured during online inspection.

4. EXPERIMENTAL RESULTS

In a practical experiment, we evaluate the illumination technique presented in the previous Section 3 on the problem of material type classification of printed circuit boards (PCBs). The automated visual inspection of PCBs is a challenging problem due to the mixture of different materials such as metals, varnishes, and substrates of which the PCB elements are composed. Numerous approaches to PCB inspection have been described in the literature, however, most of them are based on measuring the spectral reflectance of the materials by color or multispectral imaging.^{14,15} In this work, we solely use grayscale images (i.e., without color or spectral information) but evaluate angular resolved reflectance measurements to extract features for material classification.

In a training stage, we recorded an illumination series $\{g(\mathbf{x}, L_{\omega_j}^{\text{rect}}(\omega))\}_{j=1}^{60}$ of a PCB with the impulse-like basis illumination function described in Equation (6). The PCB under uniform illumination is shown in Figure 3a. It is composed of three material types: ground substrate and two different conducting elements made of silver and gold. Since we aim to classify the material into different types, we need to find a linear transformation \mathbf{W} that extracts low-dimensional reflectance features with maximum class separability from the illumination series. To this end, we utilized Fisher’s linear discriminant analysis (FDA)¹⁶ for $c = 3$ classes to compute an optimal transformation that minimizes the within-class variability and maximizes the between-class separability of the extracted features simultaneously. This is equivalent to maximizing the criterion

$$J(\mathbf{W}) = \frac{|\mathbf{W}^T \mathbf{S}_B \mathbf{W}|}{|\mathbf{W}^T \mathbf{S}_W \mathbf{W}|}, \quad (17)$$

where \mathbf{S}_B denotes the between-class and \mathbf{S}_W the within-class scatter matrix. An optimal transformation with maximal class discrimination can then be computed by applying an eigendecomposition on the scatter matrices of a labeled training data set.¹⁷ However, with FDA, the upper bound of dimensions l in the transformed feature space is $c - 1$, where c is the number of different classes. Therefore, as a result, we obtain two linear discriminant functions $\mathbf{w}_1^{\text{FLD}}$ and $\mathbf{w}_2^{\text{FLD}}$ which we encode as pairs of illumination patterns $\{L_1^{\text{FLD}^+}(\omega), L_1^{\text{FLD}^-}(\omega)\}$ and $\{L_2^{\text{FLD}^+}(\omega), L_2^{\text{FLD}^-}(\omega)\}$ as described in Section 3.2. In Figures 3b and 3c, the resulting images $g(\mathbf{x}, L_1^{\text{FLD}}(\omega))$ and $g(\mathbf{x}, L_2^{\text{FLD}}(\omega))$ of the PCB illuminated with the derived illumination patterns are shown. As described above, for each loading vector containing negative values, two illumination patterns were projected and the captured images were subtracted according to Equation (15). As a result, we were able to obtain the score image of a discriminant function by illuminating the PCB with only two illumination patterns. To illustrate the appropriateness of the score images for material classification, Figure 3d shows the joint histogram of the two score images. As can be seen, three clusters can be identified, which correspond to the three materials of the PCB.

Next, we applied the k -means clustering algorithm with $k = 3$ for unsupervised material classification to the illumination series $\{g(\mathbf{x}, L_1^{\text{FLD}}(\omega)), g(\mathbf{x}, L_2^{\text{FLD}}(\omega))\}$. The classification result is illustrated in Figure 4a, where different colors represent distinct PCB materials. In order to evaluate the performance of the proposed method, we applied a 10-fold cross-validation scheme to compare the classification results with hand-annotated ground truth data and calculated the classification accuracy from the resulting confusion matrix.¹⁸ In Figure 4b, the classification accuracy is shown for using only the first discriminant function as illumination pattern (two images need to be captured) and using both discriminant functions as illumination patterns (four images need to be captured).

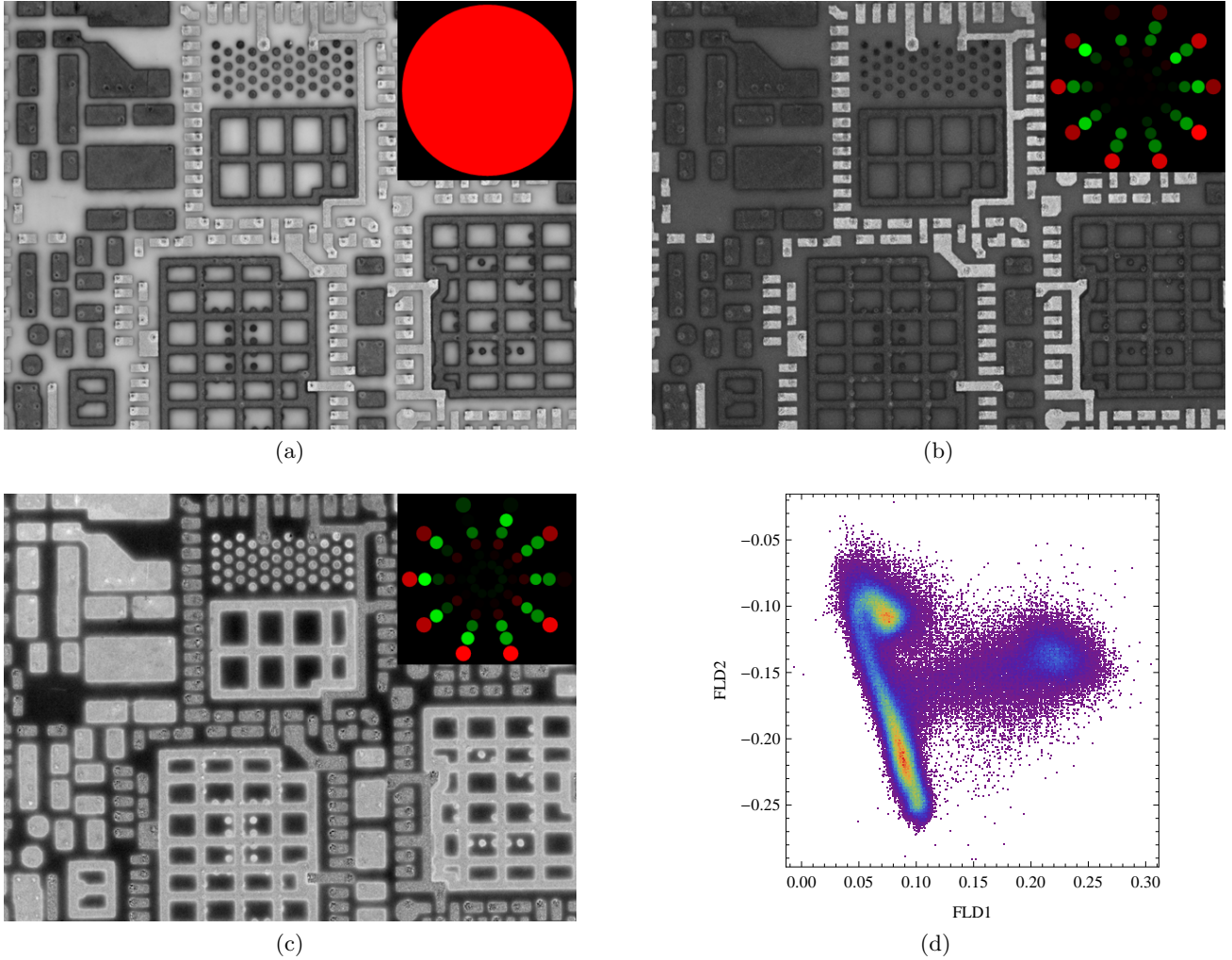
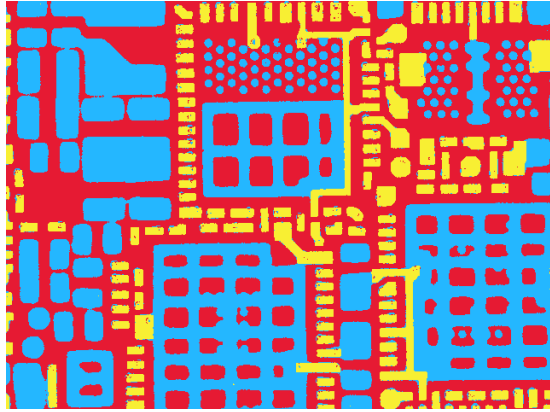
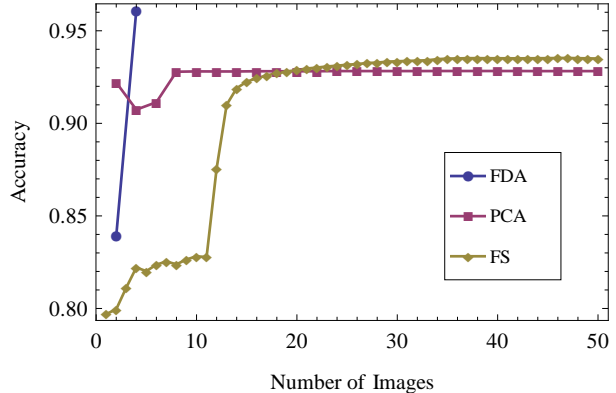


Figure 3. Images of a printed circuit board (PCB) using different illumination patterns. The illumination patterns are shown as inset, red intensities encode positive radiance values, green intensities encode negative radiance values. (a) PCB under uniform illumination. (b)-(c) Images of the PCB by encoding Fisher’s linear discriminant functions as illumination patterns. (d) Joint histogram of the images shown in (b) and (c).

In addition, the proposed FDA approach is compared to other methods for dimensionality reduction that allow deriving a set of optimal illumination patterns. In multivariate image analysis, principal component analysis (PCA) is without doubt the most frequently used method for dimensionality reduction and feature extraction.¹⁹ In contrast to FDA, PCA does not optimize the class separability of the extracted features but computes latent variables (i.e., principal components) with maximum variances that provide an optimal representation of the original variables. As such, PCA is an unsupervised technique, which does not use any class information for feature extraction. However, PCA allows extracting up to m principal components, i.e., the dimension of the transformed feature space is not limited as with FDA. In our experiments, we encoded the first 25 principal components as pairs of illumination patterns $\{L_k^{\text{PC}^+}(\omega), L_k^{\text{PC}^-}(\omega)\}_{k=1}^{25}$ and used these to sequentially illuminate the PCB. Next, k -means clustering was applied to the captured image series $\{g(\mathbf{x}, L_k^{\text{PC}}(\omega))\}_{k=1}^l$ with increasing size $l = 1, \dots, 25$. As before, the classification accuracy was calculated using ground truth data and a 10-fold cross-validation scheme. The results are shown in Figure 4b. Finally, we performed dimensionality reduction by feature subset selection (FS) to obtain a set of illumination patterns. In contrast to the preceding methods, feature selection preserves the original features and therefore, in our case, returns a subset of the basis illumination patterns $\{L_{\omega_1}^{\text{rect}}(\omega), \dots, L_{\omega_m}^{\text{rect}}(\omega)\}$. In our experiments, we used forward feature selection²⁰ to obtain



(a)



(b)

Figure 4. (a) Segmentation result using k -means clustering on the illumination series consisting of the images shown in Figure 3b and 3c. (b) Classification accuracies of the PCB test example for different illumination series. The illumination patterns for the illumination series were computed by principal component analysis (PCA), Fisher’s linear discriminant analysis (FDA) and feature forward selection (FS).

a good set of illumination patterns by greedily adding the best pattern for material classification at each step. To evaluate the performance of the individual illumination directions, we applied 10-fold cross-validation on the ground truth data set. The classification accuracy of k -means clustering for the increasing illumination series $\{g(\mathbf{x}, L_{\omega_k}^{\text{rect}}(\omega))\}_{k=1}^l$, $l = 1, \dots, 50$ is shown in Figure 4b. Note, since the basis illumination patterns solely encode positive values, no image pairs had to be captured and processed.

A comparison of the empirically derived classification accuracies in Figure 4b reveals, that the FDA computed illumination patterns significantly perform best for unsupervised material classification. Furthermore, the best performance is achieved with a very small illumination series of just four illumination patterns, which encode the two linear discriminant functions of the 3-classes classification problem. However, by restrict the number of recordable images to a limit of two, PCA provides the illumination patterns with the best classification accuracy.

5. SUMMARY AND CONCLUSION

We have presented a novel illumination technique for automated visual inspection that uses hemispherical illumination patterns to extract reflectance features directly in the optical domain. Based on the linear properties of light transport, we showed how these illumination patterns can be computed as linear combination of a set of basis illumination patterns. For this purpose, we considered illumination series as multivariate images and utilized techniques from multivariate statistics to derive linear functions for feature extraction in a separate training stage. Since the computed illumination patterns are highly problem specific, much less images have to be captured during online inspection to capture the relevant reflectance features of the object under study.

In order to experimentally evaluate the proposed illumination technique, we presented a catadioptric illumination device which is able to generate arbitrary complex illumination patterns over the hemisphere. As an application example, illumination series of a printed circuit board (PCB) were captured with different illumination patterns and used for unsupervised material classification. A comparison of the empirically derived classification accuracies revealed, that from Fisher’s linear discriminant analysis derived illumination patterns significantly perform best for material classification. In addition, the best classification result was obtained by using only four illumination patterns.

REFERENCES

- [1] Puente Leon, F., “Enhanced imaging by fusion of illumination series,” in [*Sensors, Sensor Systems, and Sensor Data Processing*], Loffeld, O., ed., **3100**, 297–308, SPIE, Munich, Germany (1997).

- [2] Lindner, C. and Puente Leon, F., “Model-Based segmentation of surfaces using illumination series,” *Instrumentation and Measurement, IEEE Transactions on* **56**(4), 1340–1346 (2007).
- [3] Wang, O., Gunawardane, P., Scher, S., and Davis, J., “Material classification using BRDF slices,” in [*Computer Vision and Pattern Recognition, IEEE Computer Society Conference on*], **0**, 2805–2811, IEEE Computer Society, Los Alamitos, CA, USA (2009).
- [4] Hastie, T., Tibshirani, R., and Friedman, J., [*The Elements of Statistical Learning: Data Mining, Inference, and Prediction, Second Edition*], Springer, 2nd ed. 2009. corr. 3rd printing ed. (2009).
- [5] Jehle, M., Sommer, C., and Jähne, B., “Learning of optimal illumination for material classification,” in [*Pattern Recognition*], Goesele, M., Roth, S., Kuijper, A., Schiele, B., and Schindler, K., eds., *Lecture Notes in Computer Science* **6376**, 563–572, Springer Berlin / Heidelberg (2010).
- [6] Gruna, R. and Beyerer, J., “Acquisition and evaluation of illumination series for unsupervised defect detection,” in [*Proc. IEEE Instrumentation and Measurement Technology Conference*], 192–197 (2011).
- [7] Horn, B. K., [*Robot Vision*], McGraw-Hill Higher Education, 1st ed. (1986).
- [8] Weyrich, T., Lawrence, J., Lensch, H. P. A., Rusinkiewicz, S., and Zickler, T., “Principles of appearance acquisition and representation,” *Foundations and Trends in Computer Graphics and Vision* **4** (Feb. 2009). ACM ID: 1640477.
- [9] Debevec, P., Hawkins, T., Tchou, C., Duiker, H. P., Sarokin, W., and Sagar, M., “Acquiring the reflectance field of a human face,” in [*Proceedings of the 27th annual conference on Computer graphics and interactive techniques*], 145–156 (2000).
- [10] Masselus, V., *A practical framework for fixed viewpoint image-based relighting*, PhD thesis, Katholieke Universiteit Leuven (2004).
- [11] Heidrich, W. and Seidel, H.-P., “Realistic, hardware-accelerated shading and lighting,” in [*Proceedings of the 26th annual conference on Computer graphics and interactive techniques*], *SIGGRAPH '99*, 171–178, ACM Press/Addison-Wesley Publishing Co., New York, NY, USA (1999).
- [12] Geyer, C. and Daniilidis, K., “Catadioptric projective geometry,” *International Journal of Computer Vision* **45**(3), 223–243 (2001).
- [13] Varmuza, K. and Filzmoser, P., [*Introduction to Multivariate Statistical Analysis in Chemometrics*], Crc Pr Inc (2009).
- [14] Ibrahim, A., Tominaga, S., and Horiuchi, T., “Spectral imaging method for material classification and inspection of printed circuit boards,” *Optical Engineering* **49**(5), 057201 (2010).
- [15] Horiuchi, T., Suzuki, Y., and Tominaga, S., “Material classification for printed circuit boards by kernel fisher discriminant analysis,” in [*Computational Color Imaging*], Schettini, R., Tominaga, S., and Tremeau, A., eds., **6626**, 152–164, Springer Berlin Heidelberg, Berlin, Heidelberg (2011).
- [16] Ripley, B. D., [*Pattern Recognition and Neural Networks*], Cambridge University Press, 1 ed. (2008).
- [17] Duda, R. O., Hart, P. E., and Stork, D. G., [*Pattern Classification: Pattern Classification Pt.1*], Wiley & Sons, 2nd ed. (2000).
- [18] Webb, A. R. and Copsey, K. D., [*Statistical Pattern Recognition*], Wiley, 3 ed. (Oct. 2011).
- [19] Geladi, P. and Grahn, H., [*Multivariate Image Analysis*], Wiley (1997).
- [20] Liu, H. and Motoda, H., [*Computational Methods of Feature Selection*], Chapman and Hall/CRC, 1 ed. (Oct. 2007).